# Vortex-Induced-Vibration of Jack-ups with Cylindrical Legs in Multiple Modes

Sudheesh Ramadasan,

Marine Technology, Newcastle University in Singapore, 537 Clementi Road #06-01, SIT@NP Building, Singapore 599493

Longbin Tao*,

Department of Naval Architecture, Ocean & Marine Engineering, University of Strathclyde, Glasgow G4 0LZ, United Kingdom

Arun Kr Dev,

Marine Technology, Newcastle University in Singapore, 537 Clementi Road #06-01, SIT@NP Building, Singapore 599493

## Abstract

A simple mathematical model was developed based on the single-degree-of-freedom analogy and principle of conservation of energy evaluating various modes of Vortex-Induced-Vibration (VIV) of a jack-up with cylindrical legs in steady flow. Mass ratio, damping ratio and mode factor were found to be the important parameters controlling the inline and cross flow VIV and radius of gyration for the yaw VIV. Criteria for the initiation of the three VIV modes were developed for the cases of a single 2D cylinder, four rigidly coupled 2D cylinders in rectangular configuration and a jack-up experiencing

* Corresponding author. Tel: +44 (0)141 548 3315; Email: longbin.tao@strath.ac.uk

uniform flow. The model tests demonstrated that the jack-up with cylindrical legs experienced cross flow and yaw VIV in uniform flows, with amplitude ratios greater than 0.1D. Further, there was considerable overlap of the lock-in ranges and coupling at higher current speeds of the aforementioned modes making the jack-up practically redundant throughout the operating currents. The analysis of the mean inline responses of the model revealed drag amplification due to the VIV. The test results validated the developed VIV model, VIV criteria and the importance of mass ratio in suppressing VIV. The mathematical method will enable practising engineers to consider the effect of VIV in jack-up designs.

Keywords, Jack-up, Vortex-induced-vibration (VIV), VIV criteria, VIV suppression

# 1. Introduction

Flow around circular cylinders is one of the extensively researched subjects in fluid mechanics. Alternate shedding of vortices about the cylinders due to flow separation can cause Vortex-Induced-Vibration (VIV), which can eventually lead to structural yield and fatigue failures. Comprehensive reviews on VIV can be found in Sarpkaya and Isaacson (1981), Blevins (2001), Sarpkaya (2004), Williamson and Govardhan (2004) and Sumer and Fredsøe (2006).

VIV in water is characterised by low mass ratio, added mass and significant fluid damping. King et al. (1973) investigated the nature of VIV in water by means of an exhaustive test programme using model piles and observed VIV along both inline and cross flow directions. Khalak and Williamson (1997a) conducted experiments with an elastically mounted rigid cylinder in water and found an upper branch of VIV with large vibration amplitudes owing to very low mass ratio and damping. It was observed that oscillation frequency kept increasing above the natural frequency throughout the excitation regime and considerable lift and drag amplification during lock-in vibrations. Khalak and Williamson (1997b) presented the results of tests performed to separately determine the effect of mass ratio and damping ratio.

It was reported that the overall range of excitation as well as the shape of the response curve is determined by the mass ratio while the level of response is characterised by the mass damping parameter. Govardhan and Williamson (2004) found that the vibration frequency during lock-in is primarily dependent on mass ratio and vibration frequency can reach remarkably large values when mass ratio is in the order of unity. The authors proposed an expression for the lower branch vibration frequency and confirmed the existence of a critical mass ratio below which the structure will vibrate till infinite flow speed in the upper branch. This revealed that the added mass of cylinders during large amplitude cross flow vibration is negative. Blevins and Coughran (2009) conducted tests on VIV of an elastically supported cylinder in water and observed that the lock-in range increased with a decrease in mass ratio and for light cylinders, the vibration frequency increased up to 50% above cylinder's natural frequency. Vandiver (2012) proposed an alternative damping parameter (C*) to overcome the limitation of mass damping parameter and argued that the alternative might be used to characterise VIV at all reduced velocities in the lock-in range and multiplied with the amplitude ratio to calculate the lift coefficient. It was also noted that inline cylinder vibrates at twice the shedding frequency.

Multi-cylinder structures are extensively used in marine and offshore industries, typical concepts being jacket platforms, semi-submersibles, riser bundles and jack-up platforms. Figure 1 displays a typical jack-up with cylindrical legs performing soil investigation. Floating multi-cylinder structures like semi-submersibles and TLPs are found to experience Vortex Induced Motion (VIM), a low frequency equivalent of VIV. The mass ratio of unity and low slenderness ratio of the cylinders can be regarded as the main difference of VIM with jack-up undergoing VIV. However, as previous studies are limited for the VIV of a jack-up, the available literature on VIM and VIV of rigidly coupled multiple cylinders can be used effectively to draw relevant insights on the former. A comprehensive review of the research developments on VIM was presented by Fujarra et al. (2012). Gonçalves et al. (2011b) conducted experimental studies on VIM with a scaled model of the semi-submersible and found that inline, cross flow and yaw motions were experienced. It was also observed lock-in for both the cross flow and yaw motions and the later was named as vortex-induced-yaw motion (VIY). It was further stated that VIY occurred when vortex shedding frequency about the columns approached the natural frequency of yaw of the semi-submersible. Liang et al. (2017) carried out a comprehensive numerical study complimented by experimental measurements on the VIM of a deep draft semi-submersibles to examine the characteristics of vortex shedding processes and their interactions due to multiple cylindrical columns. Gonçalves et al. (2018) conducted experiments on deep draft semi-submersibles models to investigate the effects of the column shape and the surface roughness. It was found that the circular column experienced higher VIM amplitudes in both transverse and yaw motions and confirmed the existence of lock-in ranges for both modes. It was also observed dynamic amplification of drag, lift and yaw moment coefficients during lock-in. Gonçalves et al. (2011a) conducted VIV experiments with cantilevered bar and pivoted pendulum of low mass and aspect ratios, and compared the results with the published literature on VIM to establish similarity between VIM and VIV. It was observed similarity in trends and values between both the phenomena and that higher aspect ratios experienced higher amplitudes due to enhanced vortex correlation.

Figure 1. Jack-up with cylindrical legs (Ms Cybermarine Technologies Pte. Ltd.)

The spacing between the cylinders is a significant parameter for multi-cylinder VIV as the cylinders are strongly influenced by wake and proximity interference effects. The flow around the downstream cylinders is highly influenced by the wake of the upstream cylinders. Sumner (2010) has presented an exhaustive review of the literature on the flow around two identical circular cylinders in a steady flow, covering the three main configurations namely tandem, side by side and staggered. Bearman (2011) has reviewed the recent research on the VIV of isolated circular cylinders and circular cylinders in tandem arrangement. Zdravkovich (1985) conducted extensive wind tunnel experiments with two identical cylinders in tandem, side by side and staggered arrangements covering the proximity interference, wake interference and no interference regions as depicted in Figure 2. Based on the experimental study, Zdravkovich (1985) concluded that the coupling between cylinders disappeared when the transverse pitch ratio was above 4, and the wake interference gradually diminished when the longitudinal pitch ratio was greater than 7. Wang et al. (2013) conducted an experimental study of flow around four circular cylinders in a square configuration and reconfirmed that depending on the pitch ratio, the inline flow can be broadly classified as shielding regime, shear layer reattachment regime and vortex impinging regime. It was observed that for transverse spacing ratios above 4, the four cylinder array could be regarded as two isolated parallel rows of two cylinders in tandem. It was further revealed that for large pitch ratios ($P/D > 5$), the vortex shedding from all four cylinders is fully synchronised with constant frequency and definite phase relationships. Assi et al. (2010) studied the wake induced vibration (WIV) response of a downstream cylinder for various longitudinal pitch ratios and found that the downstream cylinder experienced vibrations with increasing amplitudes at higher reduced velocities for the pitch ratios less than 8. For pitch ratios greater than 8, however, the WIV was seen progressively reduced, and the response amplitude peak corresponded to that of VIV resonance.

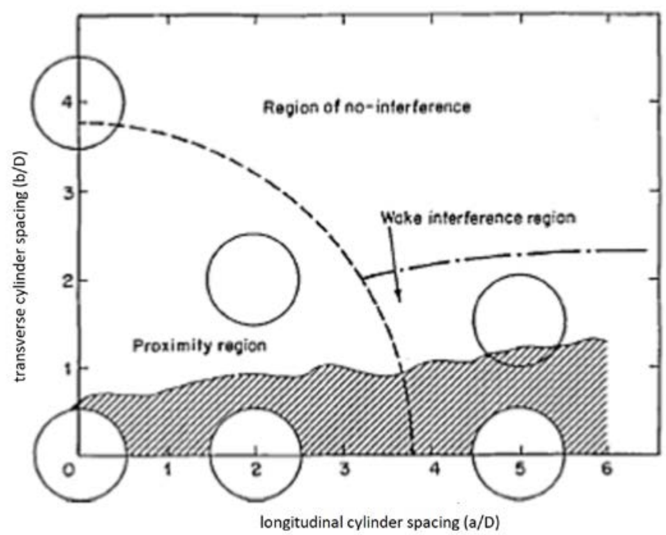


Figure 2. Cylinder interference regions (Zdravkovich, 1985)

Jiang (2012) numerically studied flow induced transverse vibrations of two tandem cylinders between two parallel walls and effect of pitch ratios ranging from 1.1 to 10. It was found that the cylinders decouple and behave as two isolated cylinders for larger pitch ratios above 8. Han et al. (2015) numerically investigated the flow induced vibration of four uncoupled identical circular cylinders in a square arrangement subjected to uniform flow. Dual resonance or cylinder synchronised vibrations were identified along both inline and cross flow directions during lock-in for a pitch ratio of 5. Zhao and Cheng (2012) performed numerical simulation of VIV of four rigidly coupled square cylinders in a square configuration with a pitch ratio of 3. It was reported that there were two modes of vortex shedding, symmetrical and synchronised. In the symmetrical mode, cylinders on either side were found to shed vortices symmetrically about the longitudinal centre line. The synchronised mode was found to cause aggressive lock-in vibrations due to the synchronisation of vortex shedding about all the four cylinders.

Self-elevating platforms or jack-ups with cylindrical legs are usually deployed in shallow and intermediate waters. Cylindrical legs, typically having diameters from 0.50m to 4.00 m can potentially lead to large resonant vibration and lock-in in lateral and yaw directions of the jack-ups when the vortex shedding frequency approaches the unit's natural frequency. Such VIV can amplify the mean drag acting on the legs, resulting in high static and cyclic stresses and eventually lead to yield and fatigue damages. Nicholls-Lee et al. (2013) pointed out the instability of the jack-ups in high tidal currents and associated VIV causing large topside motions leading to abortion of operations. Thake (2005) described the VIV experienced by jack-ups working in deep and fast currents and further stated the lack of established design guidelines to address this issue and the need for developing new methods. The potential modes of VIV of the jack-up are illustrated in Figure 3.

a) b) c)

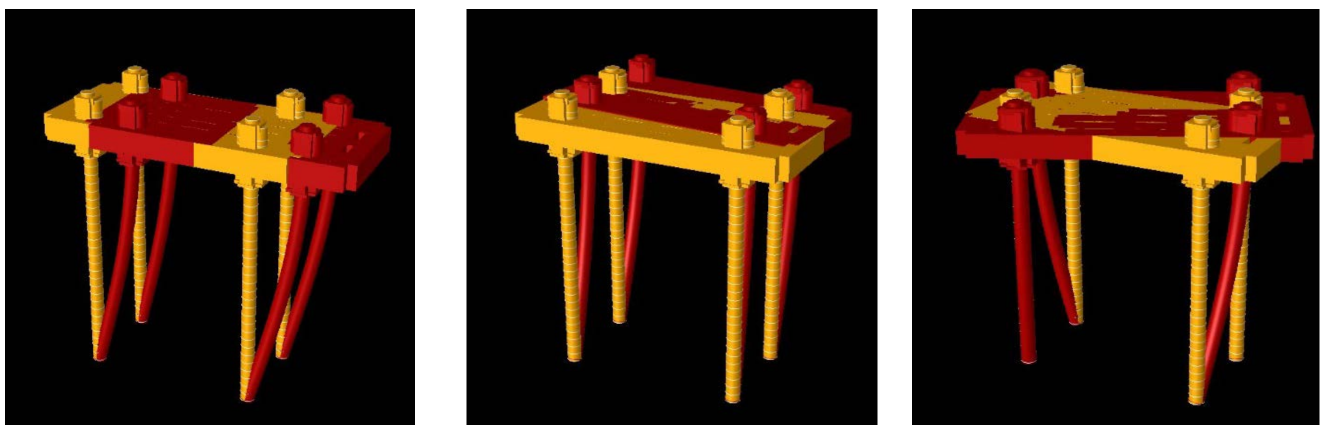

Figure 3. Jack-up VIV modes, a) inline (surge), b) cross flow (sway), c) yaw (torsional)

The harmonic model was used to develop criteria (Barltrop and Adams, 1991; Blevins, 2001) for the occurrence of VIV. It was found that various modes of VIV can be suppressed by increasing reduced damping or mass damping parameter above certain threshold values. King et al. (1973) conducted experiments on model piles in water and developed stability criteria for the occurrence of VIV; stability parameters 1.2 and 17 for inline and cross flow mode respectively. Sakai et al. (2002) conducted experimental study on cantilever cylinders with various reduced damping and confirmed the criteria of reduced damping of 1.2 in the inline direction. Vickery and Watkins (1964) derived the dependence of response amplitude on reduced damping by considering the energy balance between excitation and damping at resonance, and presented conditions of similarity between model and prototype for VIV experiments.

There are limited model test results on jack-ups available in the published literature, and almost none of them pertains to jack-up VIV. Bennett Jr and Patel (1989) tested the scaled down model of a jack-up with truss legs to understand the dynamics in regular waves and confirmed that the behaviour was similar to a classical SDOF (single-degree-of-freedom) system. Johnson and Patel (1992) and Grundlehner (1997) presented the tests carried out with the free and restrained jack-up model in the elevated condition to measure and verify the dynamic response. The results of the fixed and free tests were compared, and the dynamic amplification factor was obtained. Cammaert et al. (2014) carried out model tests of an arctic jack-up with cylindrical legs to verify the ice loads and leg sheltering factor. Journee et al. (1988) had carried out experiments with simplified jack-up models with cylindrical legs and investigated the hydrodynamic and structural nonlinearities in the fluid-structure interaction.

The main objectives of the paper are to understand the VIV of the jack-up with multi-cylindrical legs by means of model tests and to develop simple mathematical models to evaluate the various VIV modes. A set of criteria are then proposed for predicting the occurrence of the various VIV modes of jack-ups. The significance of such a simplified mathematical approach is to enable practising engineers to account for the effect of the VIV in the design stage of jack-ups. The comprehensive experimental results presented in this paper will also serve as a benchmark for the future research of jack-up VIV.

# 2. Theoretical Evaluation

## 2.1. 2D Circular Cylinders VIV in Steady Flow

### *2.1.1. Inline/ Surge VIV of a Single Cylinder*

The inline resonant response amplitude, $x_O$ of a lightly damped linear mass spring SDOF cylinder under dynamic excitations can be expressed as (Ramadasan et al., 2018),

$$x_O = \frac{F_d}{C\omega_N} \tag{1}$$

where $F_d$, $C$ and $\omega_N$ represent the amplitude of the excitation force, damping coefficient and natural angular frequency respectively. The product $C\omega_N$ is the dynamic damping stiffness and controls the resonance amplitude. The oscillatory drag excitation ($F_d$) can be expressed as,

$$F_d = \frac{1}{2}\rho C_d D U^2 L \tag{2}$$

where $\rho$, $C_d$, $D, U$ and $L$ denote the density of the fluid, oscillatory drag coefficient, diameter of the cylinder, flow velocity and length of the cylinder respectively.

The flow velocity can be expressed in terms of the Strouhal relationship as,

$$U = \frac{f_v D}{St} = \frac{\omega_v D}{2\pi St} \tag{3}$$

where $f_v$, $\omega_v$ and $St$ represent the vortex shedding frequency, vortex shedding angular frequency and Strouhal number respectively.

The damping coefficient can be expressed in terms of a damping ratio ($\zeta$) as,

$$\zeta = \frac{C}{2\sqrt{MK}} \tag{4}$$

where $M$ and $K$ represent the mass and inline stiffness respectively of the cylinder.

During inline resonance or lock-in,

$$\omega_V = \frac{\omega_N}{2} = \frac{1}{2}\sqrt{\frac{K}{M}} \tag{5}$$

Defining mass ratio ($m^*$) of a cylinder as the ratio of mass over displaced mass,

$$m^* = \frac{M}{\rho\frac{\pi}{4}D^2 L} \tag{6}$$

Substituting Equations (2) to (6) in (1), the amplitude ratio of the inline VIV response can be derived as,

$$\frac{x_O}{D} = \frac{C_d}{16\pi^3 St^2\, \zeta m^*} \tag{7}$$

It can be seen from Equation (7) that the inline response amplitude ratio of a cylinder undergoing inline VIV in a steady flow is inversely proportional to the product of mass and damping ratios. The Reynolds number (Re) dependence of the inline VIV is also visible from the presence of Strouhal number and drag coefficient in the above expression.

A criterion for the occurrence of the inline VIV can be derived by considering 1% amplitude ratio (Barltrop and Adams, 1991).

$$\zeta m^* \le \frac{25\, C_d}{4\pi^3 St^2} \tag{8}$$

Considering a Strouhal number of 0.20 and a maximum stationary cylinder oscillatory drag coefficient of 0.10 (Sumer and Fredsøe, 2006) for the practical Re range, the criterion for the inline VIV can be derived as

$$\zeta m^* \le 0.50 \tag{9}$$

### 2.1.2. *Cross flow/Sway VIV of a Single Cylinder*

During cross flow resonance or lock-in,

$$\omega_V = \omega_N = \sqrt{\frac{K}{M}} \tag{10}$$

Like inline response, the amplitude ratio of the cross flow VIV response ($y_O$) of a 2D cylinder in a steady flow can be derived as.

$$\frac{y_O}{D} = \frac{C_L}{4\pi^3 St^2\ \zeta m^*} \tag{11}$$

where $\boldsymbol{C_L}$ represents the lift coefficient of the cylinder. The equation also shows the inverse proportionality to the product of mass and damping ratios and the Reynolds number dependence of the cross flow VIV.

Similar to inline VIV, the criterion for the occurrence of the cross flow VIV can also be derived by considering a 1% amplitude ratio (Barltrop and Adams, 1991).

$$\zeta m^* \ \leq \frac{25C_L}{\pi^3 St^2} \tag{12}$$

Considering a Strouhal number of 0.20 and a maximum stationary cylinder lift coefficient of 0.85 for the practical Re range, the cross flow VIV criterion can be derived as,

$$\zeta m^* \ \leq 17.20 \tag{13}$$

*2.1.3. Yaw VIV of a system of four 2D cylinders in rectangular configuration under inline excitation*

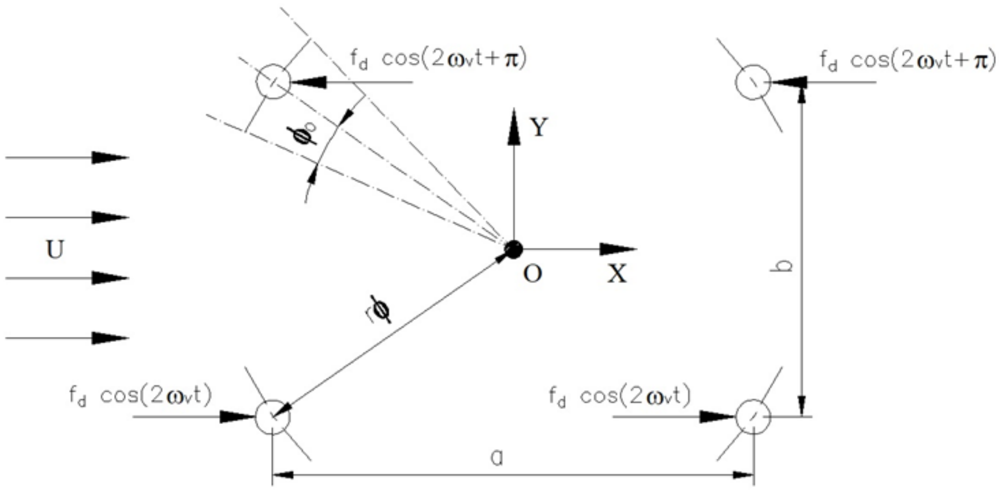


Figure 4. Yaw due to inline excitation

Like the single cylinder VIV, the amplitude of yaw VIV response ($\emptyset_O$) of a system of four 2D cylinders in a steady flow under inline or drag excitation can be expressed as,

$$\emptyset_O = \frac{M_{\emptyset O}}{C_\emptyset \, \omega_N} \tag{14}$$

where $M_{\emptyset O}$ and $C_\emptyset$ represent the amplitude of yaw excitation moment and yaw damping coefficient respectively.

The yaw excitation due to oscillatory drag, considering the vortex synchronisation between cylinders as shown in Figure 4 can be,

$$M_{\emptyset O} = 2 \times \frac{1}{2} \rho \, C_d D U^2 L \times b \tag{15}$$

where $b$ represents the cross flow or transverse cylinder spacing.

During resonance/lock-in under inline excitation,

$$\omega_V = \frac{\omega_N}{2} = \frac{1}{2}\sqrt{\frac{K_\emptyset}{I}} \tag{16}$$

where $K_\emptyset$ and $I$ represent the yaw stiffness and yaw moment of inertia respectively.

Considering the Strouhal relationship, mass ratio, damping ratio and defining the yaw radius of gyration ($\boldsymbol{r}_\emptyset$), the amplitude ratio of yaw VIV resonant response can be derived as,

$$\frac{\emptyset_O}{D} = \frac{C_d\ b}{32\ \pi^3 St^2 \zeta\ m^*\ r_\emptyset^2} \tag{17}$$

Equation (17) shows the inverse proportionality of the yaw response to the product of mass and damping ratios and the Reynolds number dependence of the yaw VIV. The proportionality with the leg transverse spacing and inverse proportionality with the square of yaw radius of gyration are also captured.

Similar to inline and cross flow VIV, considering a 1 % amplitude ratio to represent VIV occurrence,

$$\frac{r_\emptyset \emptyset_O}{D} \leq \frac{1}{100} \tag{18}$$

The criterion for the occurrence of yaw VIV under drag excitation can be derived as,

$$\zeta m^* \leq \frac{25\ C_d\ b}{8\ \pi^3 St^2\ r_\emptyset} \tag{19}$$

Considering a Strouhal number of 0.20 and a maximum stationary cylinder oscillatory drag coefficient of 0.10 for the practical Re range, the criterion becomes,

$$\zeta m^*\ r_\emptyset \leq 0.25\ b \tag{20}$$

*2.1.4. Yaw VIV of a system of four 2D cylinders in rectangular configuration under cross flow excitation.*

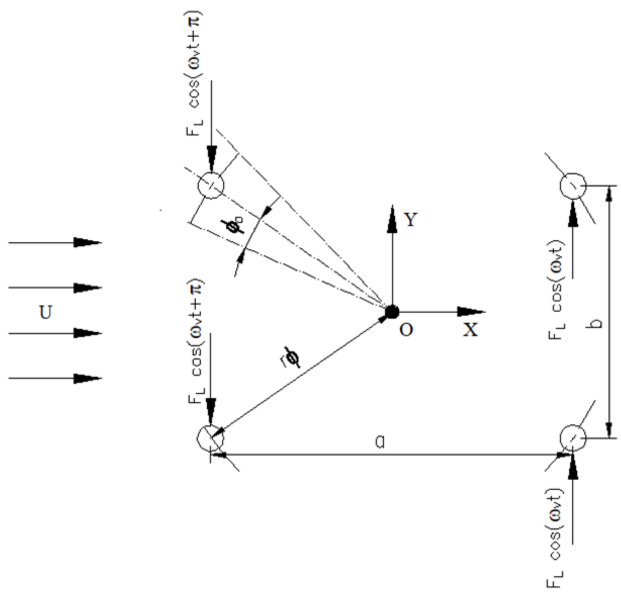


Figure 5. Yaw due to cross flow excitation

The yaw excitation due to lift, considering the vortex synchronisation between cylinders as shown in Figure 5 can be expressed as,

$$M_{\emptyset O} = 2 \times \frac{1}{2}\rho C_L D U^2 L \times a \qquad (21)$$

where $a$ is the inline or longitudinal cylinder spacing.

During resonance/lock-in under lift excitation,

$$\omega_V = \omega_N = \sqrt{\frac{K_\emptyset}{I}} \qquad (22)$$

Similar to yaw due to drag excitation, the amplitude ratio of the yaw VIV resonant response due to lift excitation can be derived as,

$$\frac{\emptyset_O}{D} = \frac{C_L\, a}{8\, \pi^3 St^2 \zeta m^*\, r_\emptyset^2} \qquad (23)$$

Equation (23) presents the inverse proportionality of the response with the product of cylinder mass ratio, damping ratios and the square of the yaw radius of gyration. Re dependence and linear proportionality with the longitudinal leg spacing are also reflected.

Similarly, the criterion for the occurrence of yaw VIV under lift excitation can be derived as,

$$\zeta m^* \leq \frac{25\, C_L a}{2\, \pi^3 St^2\, r_\emptyset} \tag{24}$$

Considering a Strouhal number of 0.20 and a maximum stationary cylinder lift coefficient of 0.85 for the practical Re range, the criterion becomes,

$$\zeta m^*\, r_\emptyset \ \leq 8.60\, a \tag{25}$$

## 2.2. VIV of Jack-up with Cylindrical Legs in Steady Flow

Figure 6 illustrates the SDOF idealisation of jack-up and the typical leg mode shape. The jack-up is idealised as an elevated concentrated mass in way of the hull leg interface with the legs providing flexural stiffness against lateral deflection.

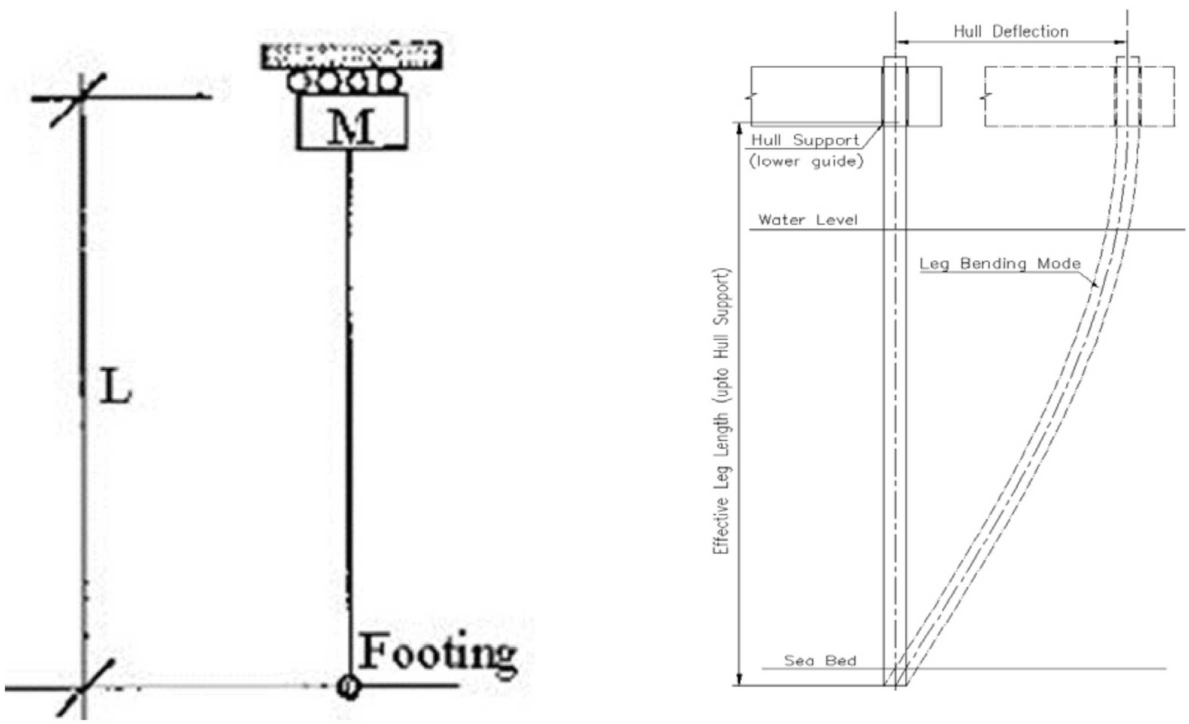


a) b)

Figure 6. Jack-up structural idealisation, a) SDOF (PANEL OC-7, 2008), b) leg mode shape

The mode shape or deflected profile of the leg of an independent leg type jack-up unit undergoing resonant vibration can be idealized as a generalised sinusoidal wave. For example, for inline vibration,

$$x_o(z) = \left[\frac{X_L}{A\,sin(k_L L+B)+E}\right][A\,sin(k_L z+B)+E] \qquad (26)$$

where $X_L$, $k_L$ represent the inline response in way of the hull interface and mode shape of the leg respectively, $A$, $B$ and $E$ are constants depending on boundary conditions and $z$ represents the elevation with respect to leg bottom with positive direction pointing upwards; at leg bottom, $z = 0$ and at hull interface, $z = L$.

The effective mass per leg ($M_{eL}$) of the equivalent single-degree-of-freedom (SDOF) system of a Jack-up idealised at the hull leg interface level can be expressed based on the energy principle (Barltrop and Adams, 1991) as,

$$M_{eL} = \int_0^L m(z) \left[\frac{A\,sin(k_L z+B)+ E}{A\,sin(k_L L+B)+ E}\right]^2 dz \tag{27}$$

where $m$ represents the mass distribution along the leg.

As evident from the Equation (27), the contributions from the individual mass components, hull, leg, entrapped mass, added mass depend on the leg mode shape and their respective locations along the leg.

### *2.2.1. Inline and Cross flow VIV*

The effective excitation force per leg ($F_{eL}$) of the SDOF system of the jack-up can be expressed based on energy principle (Barltrop and Adams, 1991) as,

$$F_{eL} = \int_0^{d'} f_O(z) \frac{A\,sin(k_L z+B)+ E}{A\,sin(k_L L+B)+ E}\, dz \tag{28}$$

where $f_O$ represents the distribution of the oscillatory excitation force along the leg.

#### *2.2.1.1. Inline / Surge VIV in Uniform Current*

The resonant inline response ($X_L$) of the SDOF can be expressed similar to Equation (1) and considering the similarity, parallelism and vortex synchronisation of the legs,

$$X_L = \frac{F_{eL}}{C_{eL}\omega_N} \tag{29}$$

where $C_{eL}$ represents the effective damping coefficient per leg.

The simplest inline VIV model for a jack-up can be developed by considering the oscillatory drag excitation as,

$$f_{Ox} = \frac{1}{2}\rho\, C_d D U^2 \tag{30}$$

where $f_{Ox}$ represents the distribution of the oscillatory drag force amplitude along the leg.

Defining the oscillatory drag force as $F_d = f_{Ox}\, d'$, Equation (29) can be simplified as,

$$X_L = \frac{F_d}{C_{eL}\,\omega_N}\left(\frac{1}{d\prime[A\,sin(k_L L+B)+E]}\right)\int_0^{d\prime}[A\,sin(k_L z + B) + E]\;dz \tag{31}$$

where $X_L$ and $d'$ represent the inline response of the leg in way of hull interface and the effective water depth considering leg penetration in the soil respectively.

Considering the Strouhal relationship, resonance/lock-in under inline excitation,

$$\frac{X_L}{D} = \frac{C_d}{16\pi^3 St^2 \zeta m^*}\left(\frac{1}{d\prime[A\,sin(k_L L+B)+E]}\right)\int_0^{d\prime}[A\,sin(k_L z + B) + E]\,dz \tag{32}$$

Equation (32) shows clearly the inverse proportionality with the mass damping parameter (product of mass ratio and damping ratio), the effect of leg mode shape and the Re dependence of the inline VIV.

Considering the 1 % amplitude ratio, the criterion for the occurrence of inline VIV of a jack-up can be derived as,

$$\zeta m^* \le \frac{25\,C_d}{4\,\pi^3 St^2}\left(\frac{1}{d\prime[A\,sin(k_L L+B)+E]}\right)\int_0^{d\prime}[A\,sin(k_L z + B) + E]\,dz \tag{33}$$

Considering a Strouhal number of 0.20 and a maximum stationary cylinder oscillatory drag coefficient of 0.10 for the practical Re range, the criterion becomes

$$\zeta m^* \left( \frac{d\prime[A\, sin(k_L L+B)+E]}{\int_0^{d\prime}[A\, sin(k_L z+B)+E] dz} \right) \leq 0.50 \quad (34)$$

The expression inside parenthesis can be defined as the mode factor (MF). The product of MF with mass damping parameter can be the effective (or modified) mass damping parameter for a jack-up. Thus the criterion becomes,

$$\zeta m^* MF \ \leq 0.50 \quad (35)$$

*2.2.1.2. Cross flow / Sway VIV in Uniform Current*

Like inline response, the cross flow response can also be derived considering Strouhal relationship and lock-in conditions as,

$$\frac{Y_L}{D} = \frac{C_L}{4\pi^3 St^2 \zeta\, m^*} \left( \frac{1}{d\prime[A\, sin(k_L L+B)+E]} \right) \int_0^{d\prime} [A\, sin(k_L z + B) + E]\, dz \quad (36)$$

where $Y_L$ represents the cross flow response of the leg in way of hull interface.

It can be observed that the inverse proportionality with mass damping parameter, the effect of leg mode shape and the Re dependence are applicable also for cross flow VIV.

Considering a 1 % amplitude ratio, the criterion for the occurrence of cross flow jack-up VIV is,

$$\zeta\, m^* \ \leq \ \frac{25\, C_L}{\pi^3 St^2} \left( \frac{1}{d\prime[A\, sin(k_L L+B)+ E]} \right) \int_0^{d\prime} [A\, sin(k_L z + B) + E]\, dz \quad (37)$$

Considering a Strouhal number of 0.20 and a maximum stationary cylinder lift coefficient of 0.85 for the practical Re range, the criterion becomes,

$$\zeta m^* MF \ \leq 17.20 \quad (38)$$

*2.2.2. Yaw VIV*

The total effective yaw excitation moment per leg ($M_{e\emptyset L}$) of the equivalent SDOF system of a Jack-up is,

$$M_{e\emptyset L} = \int_0^{d'} m_\emptyset(z) \left[\frac{A\,sin(k_L z+B)+E}{A\,sin(k_L L+B)+E}\right] dz \tag{39}$$

where $m_\emptyset$ represents the distribution of the yaw excitation moment along the leg.

The total yaw excitation on the jack-up ($M_{e\emptyset}$) can be expressed as,

$$M_{e\emptyset} = 4\, M_{e\emptyset L} \tag{40}$$

The yaw resonant response of the SDOF ($\emptyset_{\boldsymbol{L}}$) can be expressed similar to Equation (14) and considering the similarity and vortex synchronisation of the legs.

$$\emptyset_L = \frac{M_{e\emptyset}}{C_{e\emptyset}\,\omega_N} \tag{41}$$

where $C_{e\emptyset}$ represents the effective yaw damping coefficient of the jack-up SDOF.

*2.2.2.1. Yaw VIV due to inline excitation in Uniform Current*

The yaw excitation per unit leg length can be expressed as,

$$m_\emptyset(z) = f_{Ox}(z)\frac{b}{2} \tag{42}$$

where $b$ represents the cross flow or transverse spacing of legs.

Considering Strouhal relationship and lock-in condition, Equation (42) can be further simplified as,

$$\frac{\emptyset_L}{D} = \frac{C_d\, b}{32\pi^3 St^2 \zeta\, m^*\, r_\emptyset^2}\left(\frac{1}{d\prime[A\,sin(k_L L+B)+\,E]}\right)\int_0^{d\prime}[A\,sin(k_L z + B) + E] \tag{43}$$

Equation (43) shows the inverse proportionality of the yaw response with the product of cylinder mass ratio, damping ratio and the square of the yaw radius of gyration, the effect of mode shape, Re dependence and linear proportionality with the transverse leg spacing.

Considering a 1 % amplitude ratio, the criterion for the occurrence of yaw VIV of a Jack-up under drag excitation can be derived as,

$$\zeta m^* r_\emptyset^2 \le \frac{25\, C_d\, b\sqrt{a^2+b^2}}{16\, \pi^3 St^2}\left(\frac{1}{d\prime[A\, sin(k_L L+B)+E]}\right)\int_0^{d\prime}[A\, sin(k_L z+B)+E]\, dz \tag{44}$$

Considering a Strouhal number of 0.20 and a maximum stationary cylinder oscillatory drag coefficient of 0.10 for the practical Re range, the criterion becomes,

$$\zeta m^* MF\, r_\emptyset^2 \ \le 0.13\, b\, \sqrt{a^2+b^2} \tag{45}$$

The expression on the left-hand side (LHS) of Equation (45) is the product of the effective mass damping parameter and the square of the yaw radius of gyration which can be termed as the effective inertia parameter.

### *2.2.2.2. Yaw VIV due to cross flow excitation in Uniform Current*

The yaw excitation per leg is,

$$m_\emptyset(z) = f_{Oy}(z)\frac{a}{2} \tag{46}$$

where $f_{Oy}$ and $a$ represent the distribution of the oscillatory lift force amplitude along the leg and cross flow or transverse spacing of legs respectively.

Like yaw due to drag excitation, the amplitude ratio of the yaw VIV resonant response due to lift excitation can be derived as,

$$\frac{\emptyset_L}{D} = \frac{C_L\ a}{8\,\pi^3 St^2\ \zeta\ m^*\ r_\emptyset^2}\left(\frac{1}{d\prime[A\,sin(k_L L+B)+\ E]}\right)\int_0^{d\prime}[A\,sin(k_L z + B) + E]\,dz \tag{47}$$

Equation (47) shows the inverse proportionality of the yaw response with the product of cylinder mass ratio, damping ratio and the square of the yaw radius of gyration, the effect of mode shape, Re dependence and linear proportionality with the longitudinal leg spacing.

Considering a 1 % amplitude ratio to represent VIV suppression, the criterion for Yaw VIV of a Jack-up under lift excitation can be expressed as,

$$\zeta m^*\ r_\emptyset^2\ \le \frac{25\ C_L\ a\ \sqrt{a^2+b^2}}{4\,\pi^3 St^2}\left(\frac{1}{d\prime[A\,sin(k_L L+B)+\ E]}\right)\int_0^{d\prime}[A\,sin(k_L z + B) + E]\,dz \tag{48}$$

Considering a Strouhal number of 0.20 and a maximum stationary cylinder lift coefficient of 0.85 for the practical Re range, the criterion becomes,

$$\zeta m^* MF\ r_\emptyset^2\ \le 4.30\ \ a\,\sqrt{a^2 + b^2} \tag{49}$$

# 3. Physical Experiments

## 3.1. Jack-up Model

A jack-up model with a scale of 1: 28 was constructed to suit the tank dimensions. The model material was selected as PVC as per Cauchy scaling to satisfy the law of similitude for structural deflections. The leg footings were provided with ball joints to simulate the typical pinned boundary conditions. The intended elevated load was achieved by means of lead ballast plates mounted on the model deck. The elevated mass was free to vibrate in all 6 degrees of freedom (DOF) under the leg excitation. Figure 7 illustrates the jack-up model and the principal properties of the model are displayed in Table 1.

Figure 7. Jack-up model

Table 1. Model properties

| Particulars | Prototype | Model |
|---|---|---|
| Length (m) | 20.00 | 0.71 |
| Breadth (m) | 16.00 | 0.57 |
| Longitudinal Leg spacing (m) | 16.00 | 0.57 |
| Transverse Leg Spacing (m) | 12.00 | 0.43 |
| Elevated Load (kg) | 400,000 | 17.94 |
| Leg cantilever length (m) | 27.35 | 0.97 |
| Leg Diameter (m) | 0.94 | 0.034 |
| Leg Material | Mild Steel | PVC |
| Hull Material | Mild Steel | Plastic |
| Water Depth (m) | 20.00 | 0.78 |
| Wave Height (m) | 2.00 | 0.07 |
| Current (knots) | 4.00 | 0.75 |

## 3.2. Experimental Setup

The experiment was conducted in the wind wave current (WWC) tank at the Hydrodynamic Laboratory of the School of Marine Science and Technology, Newcastle University. The WWC tank has a length of 11.00 m, a width of 1.80 m and can accommodate a maximum water depth of 1.00 m, maximum wave height of 0.12 m and a maximum current of 1.00 m/s. The model was fixed to the tank bottom, positioned at the measuring section of the WWC tank and was exposed to currents with various speeds. The model was mounted on a turntable base which can be rotated to simulate various headings. The model responses were measured by means of 2 Qualisys motion tracking cameras installed on either side of the model. The experimental setup is illustrated in Figure 8.

The tank blockage is 3.78%, and the distance of the model leg from the nearest side wall is around 20 times its diameter. This ensures insignificant flow blockage and boundary effects on the test results (Chakrabarti, 2005). The scale effect due to the difference in model and prototype Reynolds numbers is expected to be minimal due to the free vibrations of the legs, as even small vibrations tend to synchronise vortex shedding and separation points (DNV.GL, 2017). Moreover, the Reynold's number influence experienced by a smooth stationary cylinder in an incoming laminar flow is not significantly felt in real flows with substantial incoming turbulence, as verified with full scale submarine pipelines and piles experiencing aggressive cross flow VIV even in critical and supercritical regimes (Raven et al., 1985; Sainsbury and King, 1971). The full scale conditions around a jack-up leg are usually influenced by a reasonable surface roughness due to the presence of marine growth (PANEL OC-7, 2008). The high turbulence intensity of around 13% generated by the inlet grid ensures a turbulent boundary layer during test conditions in the subcritical flow regime, similar to the realistic prototype conditions (Chakrabarti, 2005).

Figure 8. Experimental setup

## 3.3. Test Procedure

The tests involved mass tests, stiffness tests, free decay test and response tests. Mass tests yielded the mass, inertia and centre of gravity (COG) details of the model. Stiffness tests verified the stiffness of the model, the effect of ball joint friction on the model stiffness and associated nonlinearities. Natural frequencies, damping properties and the dynamic nonlinearities of the models were established with the free decays tests. Response tests were carried out to evaluate the modes, amplitudes and frequencies of the VIV responses experienced by the model. It is noted that response tests were carried out both in uniform current and wind to verify the effect of mass ratio and to validate the criteria developed. In order to capture all the operational envelope of a jack-up, response tests were conducted for three water depths and three elevated loads. The effect of the VIV on the mean drag force acting on the model was also established with the response tests. The details of the test cases are presented in Table 2.

Table 2. Test Matrix

| Test Case | Description | Hull Mass (kg) | Fluid Medium | Water Depth (m) | Effective Water Depth (m) |
|---|---|---|---|---|---|
| NVL, Dry | No Variable Load | 10.65 | Air | - | - |
| VL, Dry | Full Variable Load | 18.05 | Air | - | - |
| VL, 500WD | Full Variable Load | 18.05 | Water | 0.50 | 0.39 |
| VL, 700WD | Full Variable Load | 18.05 | Water | 0.70 | 0.59 |
| NVL, 890WD | No Variable Load | 10.65 | Water | 0.89 | 0.78 |
| RVL, 890WD | Reduced Variable Load | 14.08 | Water | 0.89 | 0.78 |
| VL, 890WD | Full Variable Load | 18.05 | Water | 0.89 | 0.78 |

# 4. Results and Discussion

## 4.1. Stiffness Tests

Figure 9a) illustrates the sway stiffness test setup and 9b) demonstrates the variation of sway stiffness with the deflection for the test case NVL, 890WD. It is observed that the ball joint friction was influencing the rotational fixity of the leg footing. Leg bottom behaved as a fixed footing for very small initial deflections and for reasonably large deflections as pinned footing. The model stiffness was also found to reduce during unloading cycle due to the reversal of ball joint friction. The mentioned behaviours are illustrated in the stiffness variations in Figure 9b), which also demonstrates the corresponding dynamic sway stiffnesses for the port (P) and starboard (S) sides, derived from the free decay tests. It can be observed that the dynamic stiffness is less dependent on the deflection and nearly corresponds to that of pinned footing. The surge and sway stiffnesses were found to be identical as expected due to the symmetric configuration. Yaw stiffness tests also exhibited footing fixity at very small deflections similar to the surge and sway results.

## 4.2. Free Decay Tests

Free decay tests were carried out with the model in air as well as in still water. The tests were intended to establish the natural frequency, added mass, damping and the nonlinearities of the system. As the model was found to exhibit softening nonlinearity at large deflections due to the ball joint friction or support rotational stiffness, the free decay time series was truncated to remove large amplitudes, and Fast Fourier Transform (FFT) analysis was carried out to establish the natural frequencies. The added mass of the legs was calculated from the differences in the natural frequencies of the model in air and water. The variation of the damping factor with the natural frequencies was calculated from the successive amplitude decays, and the trend was used to calculate the damping ratio corresponding to the initial natural frequency.

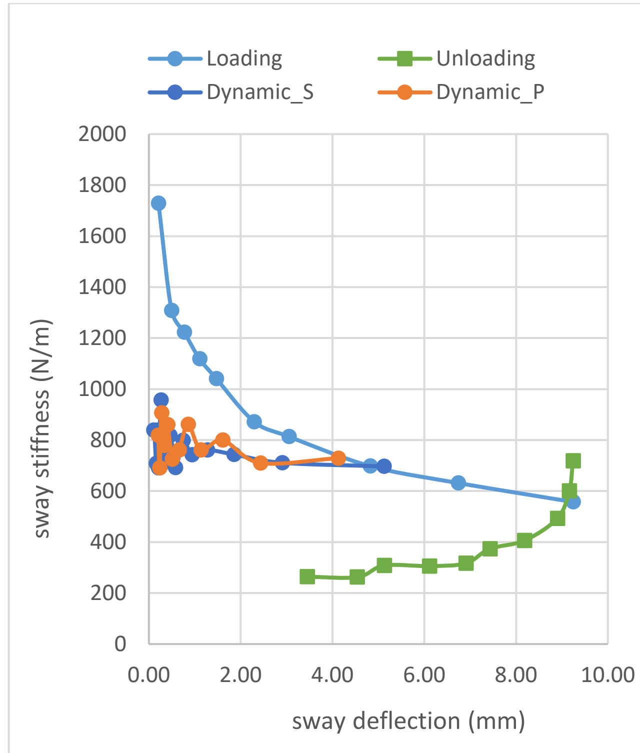


a) b)

Figure 9. a) Sway stiffness test setup b) Sway stiffness variation with deflection for NVL, 890WD

Figure 10 illustrates the results of the sway free decay test of the model for the test case, NVL, 890WD. Figure 10)a, 10)b and 10)c displays the result of FFT of the truncated histogram, the variation of the natural frequency with sway deflections and the variation of the damping ratio with the natural frequency. It was found that the damping of the model increases with reducing the natural frequency or increasing vibration amplitudes. However, it is worth noting that the damping ratios obtained from the tests were found to exhibit considerable scatter owing to the ball joint friction which influenced the results as dry friction or coulomb damping.

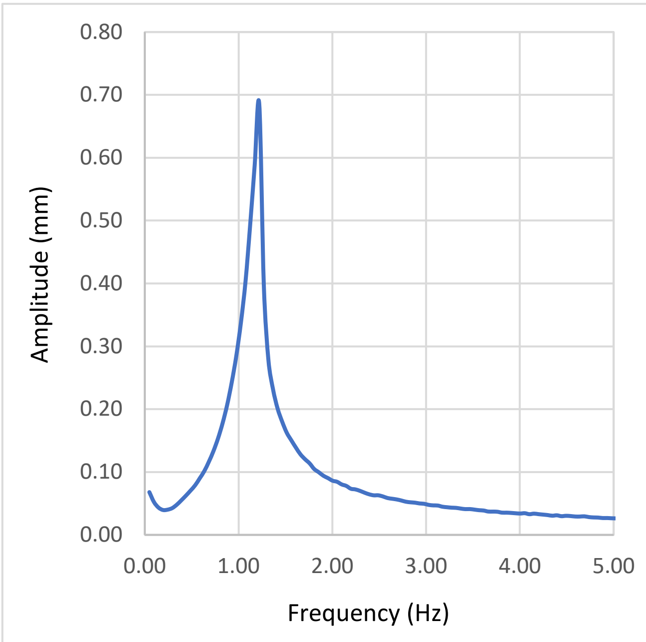


a)

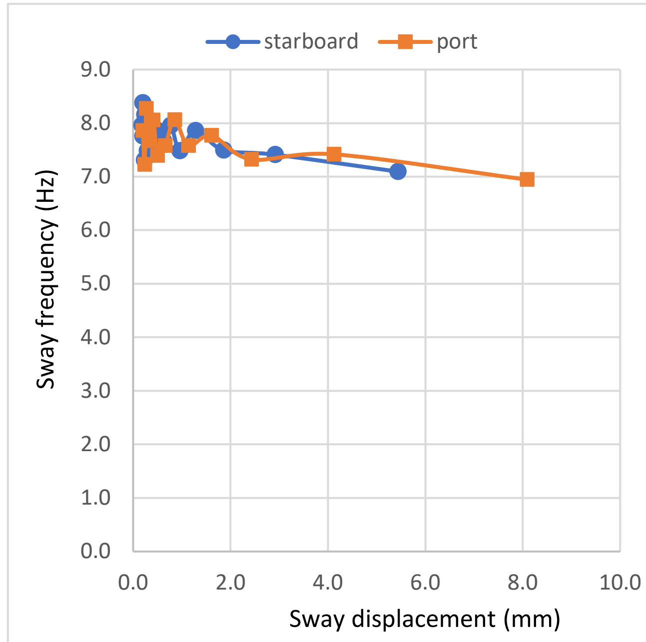


b)

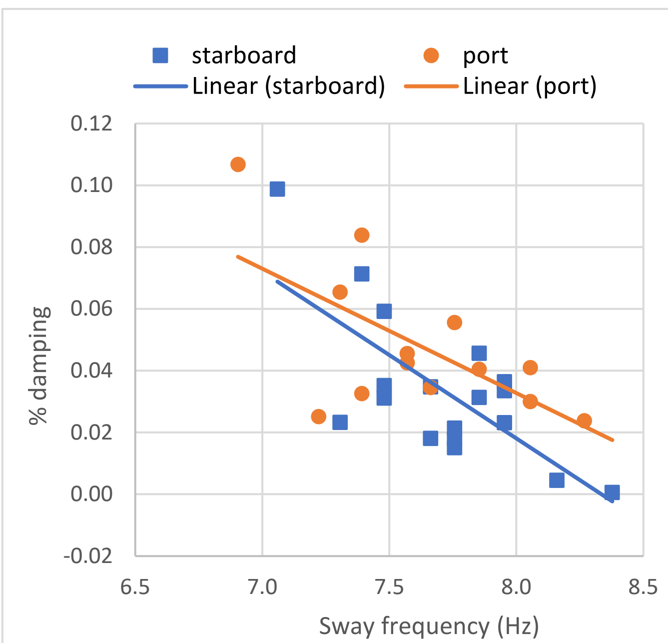


c)

Figure 10. a) FFT of sway free decay test; NVL, 890WD b) Sway natural frequency variation with displacement; NVL, 890WD c) Variation of sway damping ratio with sway frequency; NVL, 890WD.

Tables 3 and 4 summarise the results of sway and yaw free decay tests respectively. From free decay tests, the added mass coefficient of the legs in still water was found to be around 1, approaching the theoretical value. The corresponding mode shape was found to be that of pinned footing. This showed that for the practical vibration amplitudes, the model legs were vibrating with a mode shape near to that of pinned footing and the effect of the ball joint friction was negligible. It was also revealed that the damping of the system had increased in still water due to the additional fluid damping.

Table 3. Model natural frequency, added mass and damping from sway free decay tests

| Sway | | | | | | | |
|---|---|---|---|---|---|---|---|
| **Test Case** | **Damping Ratio** | **Natural Frequency (Hz)** | **Natural Period (s)** | **Added Mass (kg)** | **Leg Added Mass Coefficient** | **Fluid Damping (Ns/m)** | **Fluid damping ratio** |
| NVL, Dry | 0.036 | 1.37 | 0.73 | 0.00 | - | 0.00 | 0.00 |
| VL, Dry | 0.031 | 1.03 | 0.97 | 0.00 | - | 0.00 | 0.00 |
| VL, 500WD | 0.041 | 1.00 | 1.00 | 0.12 | 0.71 | 2.09 | 0.01 |
| VL, 700WD | 0.035 | 0.98 | 1.02 | 0.56 | 1.06 | 1.00 | 0.00 |
| NVL, 890WD | 0.040 | 1.22 | 0.82 | 1.46 | 1.35 | 1.15 | 0.01 |
| RVL, 890WD | 0.044 | 1.08 | 0.93 | 1.40 | 1.29 | 2.87 | 0.01 |
| VL, 890WD | 0.038 | 0.95 | 1.05 | 1.19 | 1.10 | 1.97 | 0.01 |

Table 4. Model natural frequency, added mass and damping from yaw free decay tests

| Yaw | | | | | | | |
|---|---|---|---|---|---|---|---|
| **Test Case** | **Damping Ratio** | **Natural Frequency (Hz)** | **Natural Period (s)** | **Added Mass Inertia ($kgm^2$)** | **Leg Added Mass Coefficient** | **Fluid Damping (Nms/rad)** | **Fluid damping ratio** |
| NVL, Dry | 0.037 | 2.05 | 0.49 | 0.00 | - | 0.00 | 0.00 |
| VL, Dry | 0.040 | 1.91 | 0.52 | 0.00 | - | 0.00 | 0.00 |
| VL, 500WD | 0.041 | 1.86 | 0.54 | 0.02 | 1.00 | 0.04 | 0.00 |
| VL, 700WD | 0.042 | 1.78 | 0.56 | 0.07 | 1.00 | 0.10 | 0.00 |
| NVL, 890WD | 0.038 | 1.81 | 0.55 | 0.13 | 0.88 | 0.11 | 0.00 |
| RVL, 890WD | 0.043 | 1.74 | 0.58 | 0.14 | 0.95 | 0.21 | 0.01 |
| VL, 890WD | 0.043 | 1.72 | 0.58 | 0.12 | 0.82 | 0.15 | 0.01 |

Table 5 displays the mass ratio, mode factor, effective mass damping parameter and effective inertia damping parameter of the model for the respective test cases. It can be inferred from the VIV criteria in Equations (35), (38), (45) and (49) that model will not experience any of the VIV modes in wind, owing to high effective mass and inertial damping parameters in the air. Further, the model is expected to experience cross flow VIV and yaw VIV due to cross flow excitation during all the test cases in water. By comparing the effective mass damping and inertia damping parameters, it is expected that the responses increase with increasing water depth and will be highest for the lightest test case, ‘NVL, 890WD’.

On verifying against the VIV criteria in Equations (35), it can be noted that the model is expected to experience inline VIV only for the lightest two test cases, ‘RVL, 890WD’ and ‘NVL, 890WD’ at 0.89m water depth. Similarly, verification against Equation (45) reveals that the model is expected to experience yaw VIV due to inline excitation for all the three test cases at 890m water depth. However, it can be deciphered that the Re corresponding to the inline VIV and yaw VIV due to inline excitation for the test cases in water is around 3000 to 5000, and the corresponding stationary cylinder oscillatory drag coefficient is 0.06 (Barltrop and Adams, 1991) that is considerably less than the upper limit value of 0.10 considered in Equation (35) and (45). On proportionally correcting the right hand side (RHS) of the equations and verifying against Table 5, it can be observed that the model will not be vulnerable to inline VIV and yaw VIV due to inline excitation in any of the test cases.

## 4.3. Response Tests

Response tests were carried out by exposing the model to incremental current from the zero heading (0 degree angle of attack). Three drafts and three loading conditions were considered for the tests to cover the realistic operation scenarios and the practical ranges of the mass ratio and the mass damping parameter. The responses of the hull along the 6 DOF were measured and recorded as individual time series. The inline, transverse and yaw time series were post processed, and the root-mean-square (rms) amplitudes and vibration frequencies were calculated for various current speeds. The results of the response tests are also summarised in Table 5.

Table 5. Response test results, a) cross flow/sway b) yaw

a)

| Sway | | | | | | | |
|---|---|---|---|---|---|---|---|
| **Case** | **m*** | **MF** | **$\zeta$** | **m*$\zeta$ MF** | **$V_{ry}$** | **$y_{O,\,rms}/D$** | **$y_{O,\,max}/D$** |
| VL, Dry | 6719.10 | 1.571 | 0.031 | 328 | 4.80 | 0.00 | 0.00 |
| VL, 500WD | 13.65 | 3.274 | 0.041 | 1.82 | 4.80 | 0.02 | 0.03 |
| VL, 700WD | 9.38 | 2.276 | 0.035 | 0.75 | 4.92 | 0.04 | 0.06 |
| VL, 890WD | 7.38 | 1.812 | 0.038 | 0.51 | 5.05 | 0.06 | 0.10 |
| RVL, 890WD | 5.96 | 1.812 | 0.044 | 0.47 | 4.82 | 0.07 | 0.11 |
| NVL, 890WD | 4.73 | 1.812 | 0.040 | 0.34 | 4.84 | 0.08 | 0.13 |

b)

| Yaw | | | | | | | | |
|---|---|---|---|---|---|---|---|---|
| **Case** | **m*** | **MF** | **$\zeta$** | **$r_\phi$ (m)** | **m*$\zeta$ MF $r_\phi^2$ ($m^2$)** | **$V_{r\phi}$** | **$R_\phi\phi_{O,\,rms}/D$** | **$R_\phi\phi_{O,\,max}/D$** |
| VL, Dry | 6719.10 | 1.571 | 0.040 | 0.215 | 19.2911 | 4.96 | 0.00 | 0.00 |
| VL, 500WD | 13.65 | 3.274 | 0.041 | 0.218 | 0.0863 | 4.96 | 0.02 | 0.04 |
| VL, 700WD | 9.38 | 2.276 | 0.042 | 0.224 | 0.0447 | 5.40 | 0.04 | 0.08 |
| VL, 890WD | 7.38 | 1.812 | 0.043 | 0.233 | 0.0310 | 5.15 | 0.07 | 0.13 |
| RVL, 890WD | 5.96 | 1.812 | 0.043 | 0.252 | 0.0293 | 5.54 | 0.06 | 0.12 |
| NVL, 890WD | 4.73 | 1.812 | 0.038 | 0.275 | 0.0245 | 5.32 | 0.06 | 0.11 |

### *4.3.1. Inline and Cross flow VIV*

Figure 11 and 12 show the variation of the normalised inline and cross flow rms amplitude responses respectively, plotted with respect to the corresponding reduced velocities. It is observed that the model does not exhibit inline VIV response for any of the test cases as predicted and evident in Figure 11. This validated the mathematical model, inline VIV criteria, and the effect of high inherent mass ratios of the jack-ups. These results demonstrated the significance of the effective mass damping parameter in suppressing VIV.

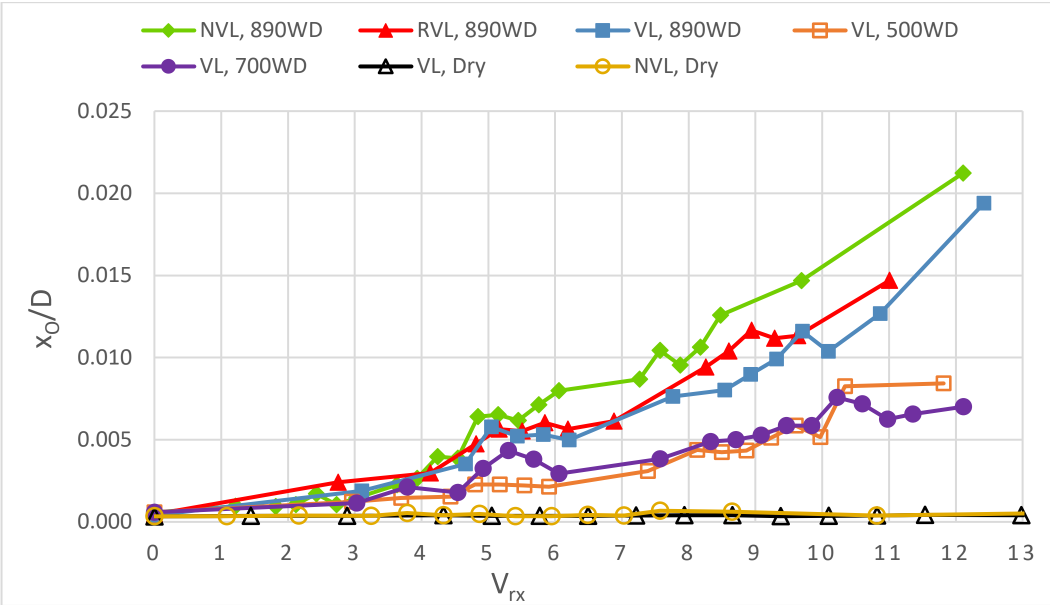


Figure 11. Inline amplitude response with corresponding reduced velocity ($U/f_{Nx}D$)

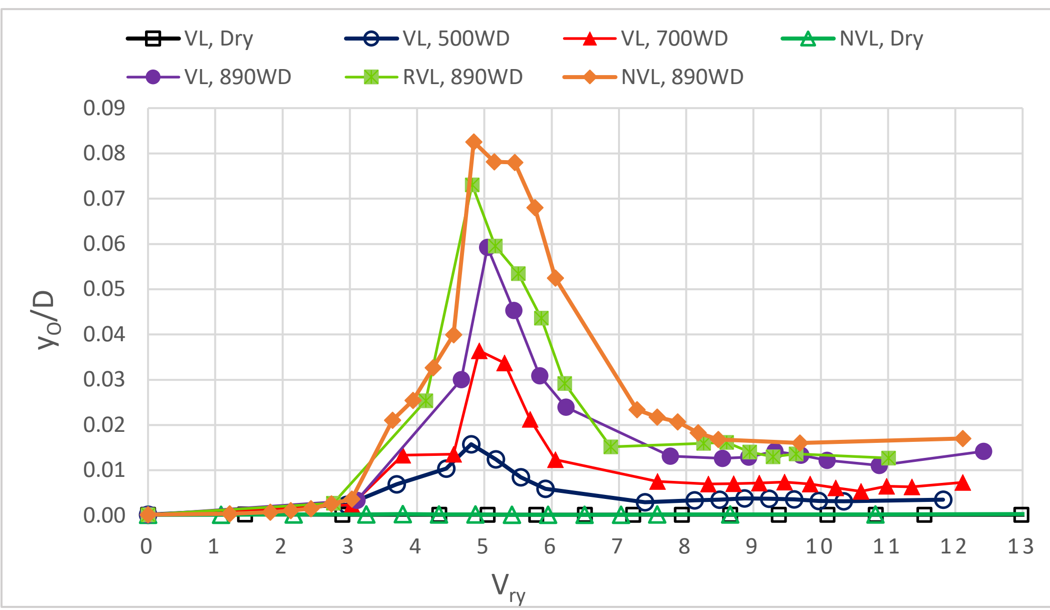


Figure 12. Cross flow amplitude response with corresponding reduced velocity ($U/f_{Ny}D$)

Figure 12 evidently shows that the model was highly vulnerable to cross flow VIV with large lock-in regimes. The response amplitudes (rms) were found to be around 0.08D, and the maximum response amplitude was observed to be as high as 0.13D. The sway lock-in regime was found to extend between reduced velocities of 3 to 8. Further, the response amplitude and lock-in range were found to increase with the increase in water depth and reduction in elevated load, with the lightest test case exhibiting the largest cross flow response amplitude and lock-in regime.

However, it is noted that the model does not exhibit any cross flow VIV during the response tests in wind. This validated the cross flow VIV criterion, the mathematical model and revealed the significance of the mass ratios in containing the VIV of the jack-ups. It was observed that the increase in mass ratio reduces the amplitude response and the lock-in range. The normalised cross flow rms response amplitude ratios fitted reasonably well in a straight line when plotted against the inverse of the effective mass damping parameter as shown in Figure 13. This further demonstrated the significance of the effective mass damping parameter in controlling the cross flow VIV response. Thus, the effective or modified mass damping parameter can be considered as the universal parameter for the comparison of cross flow VIV across various mode shapes and water depths.

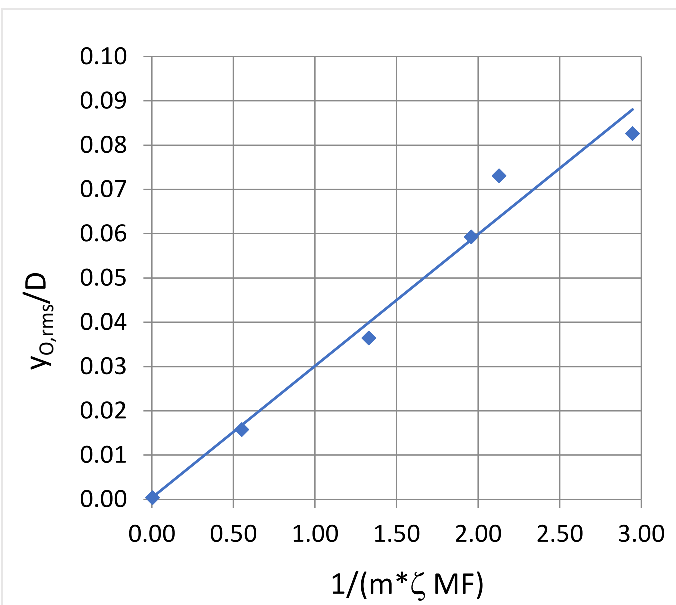


Figure 13. Cross flow amplitude response with the inverse of modified mass damping parameter.

The frequency responses of the models were calculated from the time series, normalised with the respective natural frequencies and plotted against the corresponding reduced velocities. Figure 14 illustrates the cross flow frequency responses of the model for all the test cases. It can be clearly observed that there exists two separated lock-in regimes, i.e., a lower regime with a frequency ratio of around unity and an upper regime with a frequency ratio of above 1.40. In comparison with Figure 12, it is clear that the lower regime corresponds to the cross flow lock-in responses in the sway mode while the upper regime corresponded to lock-in responses in the yaw or torsional mode. It is noted that the cross flow vibrations in the upper regime are coupled vibrations with the yaw lock-in frequencies. The coupling is evidently strong and continuous for the lightest test case but weak and intermittent for the other cases.

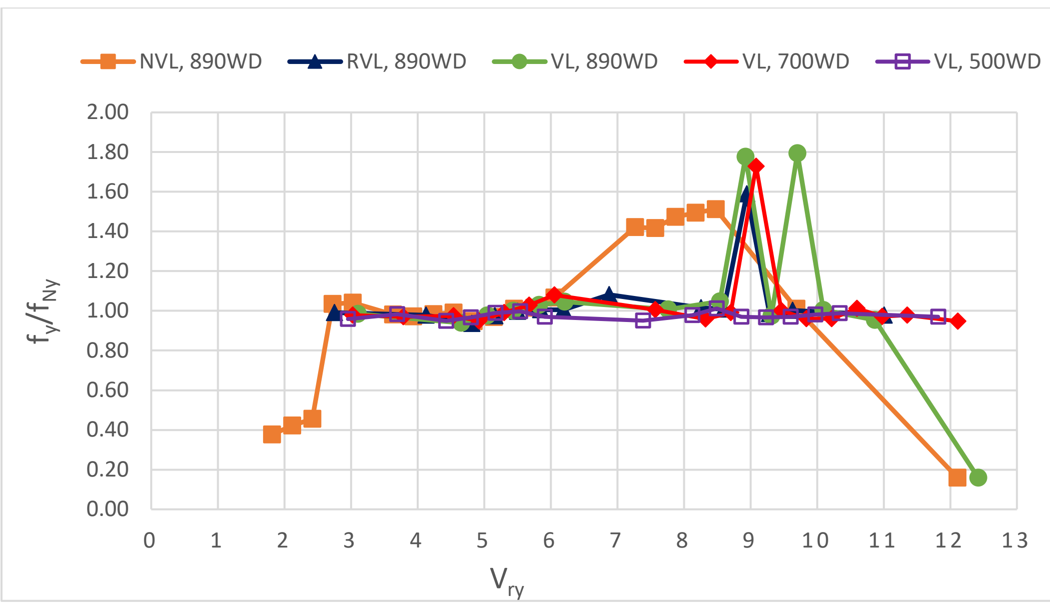


Figure 14. Cross flow frequency response with corresponding reduced velocity ($U/f_{Ny}D$)

### *4.3.2. Yaw VIV*

Experimental observation revealed that the model jack-up experienced torsional or yaw VIV response about the vertical axis at higher flow speeds. The yaw amplitude response as a function of yaw reduced velocity is plotted in Figure 15. It can be seen that the peak yaw response occurs around a yaw reduced velocity of 5, which demonstrates that the yaw VIV is due to cross flow lift excitation. The rms response amplitudes are found to be around 0.07D, and the maximum response amplitude is around 0.13D. The lock-in regime is found to extend between the yaw reduced velocities of 3 to 7. Yaw VIV due to inline excitation was not observed in any of the test cases as anticipated, validating the respective yaw VIV criterion and the mathematical model.

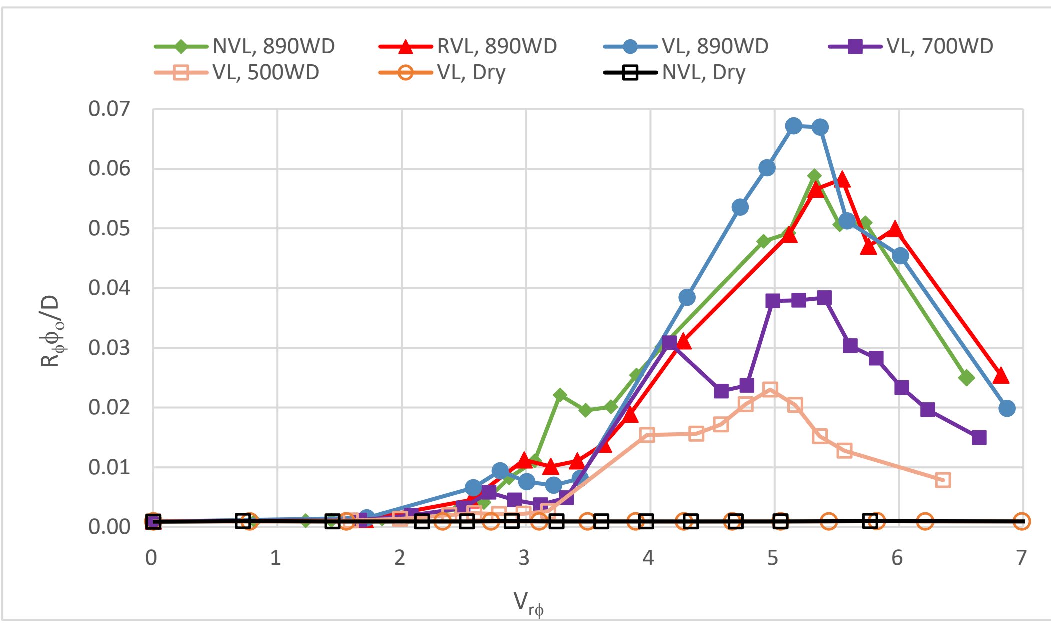


Figure 15. Yaw amplitude response with corresponding reduced velocity ($U/f_{N\phi}D$)

The response amplitude and lock-in range are found to increase generally with an increase in water depth. However, amplitude and lock-in range do not increase with the reduction in elevated load, with the response amplitudes displaying saturation in the lighter test cases. This behaviour may be attributed to the increase in yaw radius of gyration of the model with decreasing elevated load, increase in the range of overlapping sway vibrations and enhanced frequency coupling of sway with yaw vibrations with the reduction in mass ratio. Hence further experiments are necessary with model experiencing pure yaw vibrations and restrained along the cross flow direction.

It is noted that the model did not exhibit any yaw VIV either, as anticipated during the response tests in wind demonstrating the validity of the mathematical model and the significance of the mass ratios in containing the VIV of the jack-ups. It was observed that the increase in mass ratio reduces the amplitude response and the lock-in range except for the test cases at maximum water depth. The response amplitude ratio fitted reasonably well in a straight line except for the lighter test cases, when plotted against the inverse of the effective inertia damping parameter as illustrated in Figure 16. Effective inertia damping parameter is the product of mass damping parameter, mode factor and square of yaw radius of gyration, which can be considered as the universal parameter determining the yaw VIV response.

The yaw frequency responses of the model normalised with the corresponding natural frequencies and plotted against the yaw reduced velocities are displayed in Figure 17. Similar to cross flow frequency response, the yaw frequency response of the model also revealed two separated lock-in regimes, a lower regime with a frequency ratio below 0.70 and an upper regime with a frequency ratio of around 1. In comparison with Figure 14 and Figure 15, it can be seen that the lower regime corresponds to the coupled yaw vibrations in cross flow sway lock-in regime and the upper regime represents lock-in responses in the yaw mode.

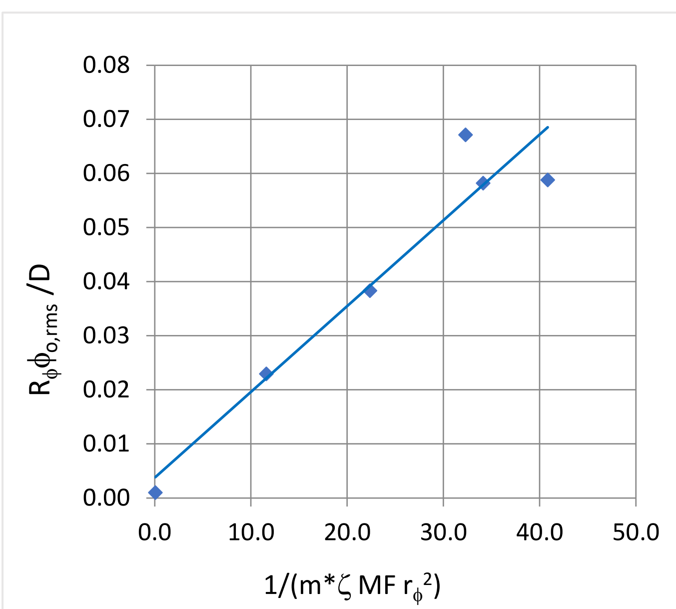

Figure 16. Yaw amplitude response with the inverse of effective inertia damping parameter

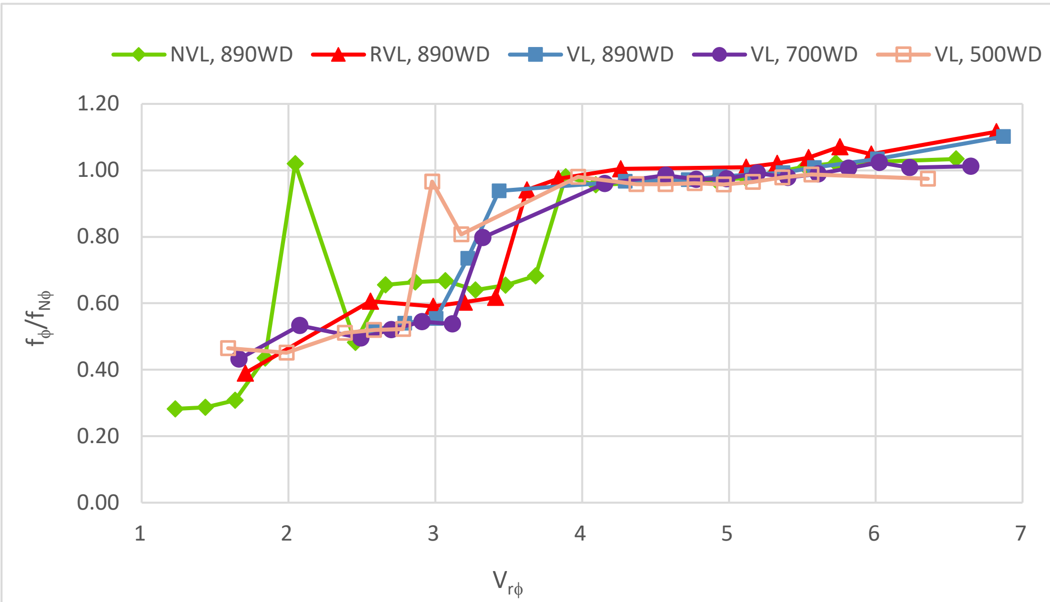


Figure 17. Yaw frequency response with corresponding reduced velocity ($U/f_{N\phi}D$)

### *4.3.3. Combined Response*

The combined cross flow amplitude response of the leg derived from the corresponding cross flow and yaw responses is plotted in Figure 18. It is found that the range of the yaw response overlaps with that of the cross flow response particularly for low mass ratios, causing a combined lock-in range throughout the operating current speeds. The combined vibrations experienced higher response amplitudes than the individual values, especially for low mass ratios. Further the combined lock-in range is seen extending almost throughout the operating current range (0.10 m/s to 0.40 m/s) making the jack-up practically redundant.

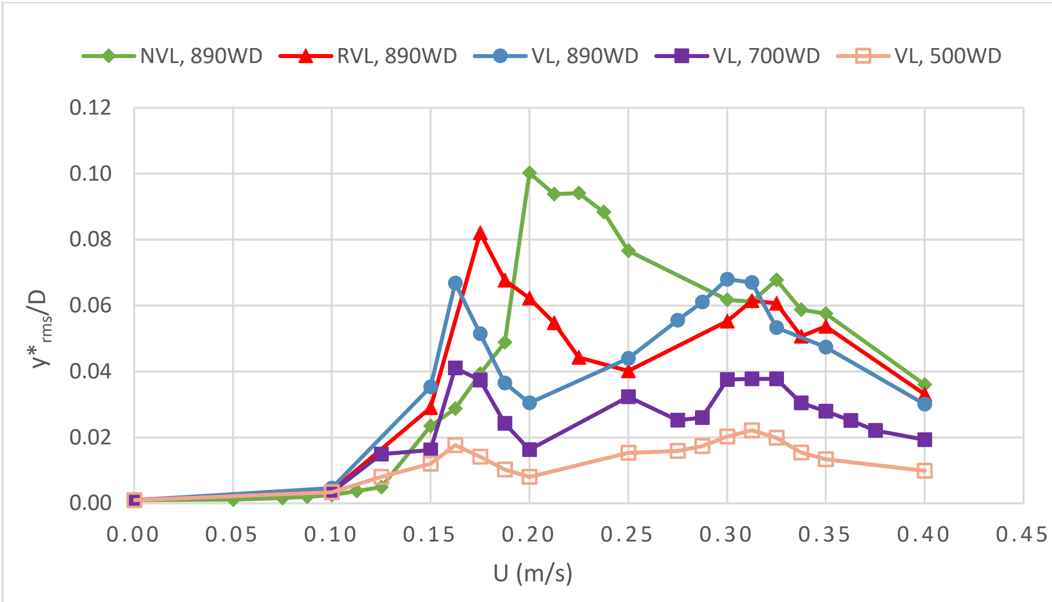


Figure 18. Leg cross flow combined amplitude response due to sway and yaw with current

### *4.3.4. Mean Response*

The mean or steady inline responses were also measured as a function of current speeds, and the normalised results were plotted in Figure 19. It can be observed that the mean inline response approximately follows a quadratic variation with the flow speeds and hence can be considered as a good representation of the drag force acting on the jack-up. The lightest operating condition (NVL, 890WD) at the maximum water depth exhibited the highest mean inline response despite having a greater stiffness due to lesser P delta effect. It is evident that the jack-up VIV increases the mean inline responses at all practical speed ranges, clearly indicating an amplification of the mean drag acting on the legs. On the other hand, the mean cross flow and yaw responses were found to be insignificant throughout the tested current speeds.

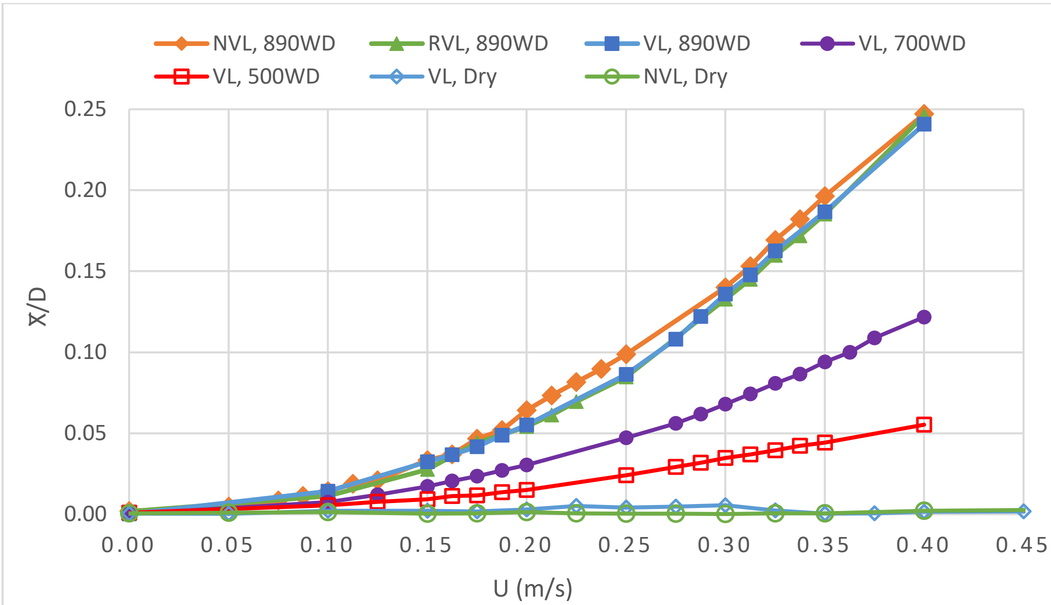


Figure 19. Inline mean response of the model with current

## 4.4. Recommendations

Based on the test results, it is recommended that the mass ratio of the jack-ups shall be as high as possible to minimise any potential VIV occurrence. Since the combined lock-in range of both the modes extends over almost all the practical current speeds, VIV and mean drag amplification can have a considerable effect on the yield and fatigue strength of the structure. Hence, necessary modifications to the present classification rules or guidelines are warranted to adequately account for the effect of VIV in the design of jack-ups.

# 5. Conclusions

A simple mathematical model was developed based on the single-degree-of-freedom analogy and the principle of conservation of energy, which can be used to evaluate various modes of VIV of a jack-up with cylindrical legs in steady flow. Mass ratio, damping ratio and mode factor were found to be the important parameters controlling the inline and cross flow VIV of jack-ups. The radius of gyration was found to be an additional important parameter influencing yaw VIV. Criteria for the occurrence of inline, cross flow and yaw VIV were developed for the cases of a single 2D cylinder, four 2D cylinders in rectangular configuration and a complete jack-up with cylindrical legs in steady uniform flow.

The model tests demonstrated that the jack-up experienced both cross flow and yaw lock-in vibrations due to lift excitation, with maximum amplitude ratios in excess of 0.1D. The jack-up was found not to experience inline and yaw VIV due to oscillatory drag excitation. Experiments conducted in wind revealed that the jack-up was not experiencing any of the VIV modes and lock-in vibrations. The observed behaviours validated the newly developed VIV model, criteria and the importance of various parameters.

From the test results, it can be inferred that the jack-ups were highly vulnerable to cross flow VIV with large lock-in ranges in light operating conditions at high water depths. Further, the lock-in range of the cross flow VIV was found to overlap with the lock-in range of yaw VIV, particularly in light operating conditions making the unit almost redundant throughout the operating current ranges. The cross flow and yaw VIV were also observed to couple at higher current speeds causing very high combined leg amplitude response. From the mean inline displacements, it was also revealed that both the cross flow and yaw VIV increases the mean drag force acting on the jack-up.

The mathematical approach presented will enable practising engineers to effectively consider the effect of VIV in jack-up designs. The test results also underline the significance of yaw or torsional VIV in the case of rigidly coupled multi-cylinder structures.

# 6. Acknowledgement

This work was carried out by using the facilities at the School of Marine Sciences and Technology, Newcastle University, UK and was supported by M/s Cybermarine Technologies Pte Ltd, Singapore. The authors gratefully acknowledge the unconditional support provided by both Newcastle University and Cybermarine Technologies.

# 7. Nomenclature

| | | |
|---|---|---|
| $a$ | = | longitudinal or inline spacing of cylinders/legs |
| $b$ | = | transverse or cross flow spacing of cylinders/legs |
| $C_L$ | = | lift coefficient |
| $C$ | = | damping coefficient |
| $C_d$ | = | oscillatory drag coefficient |
| $C_\emptyset$ | = | yaw damping coefficient |
| $C_{eL}$ | = | effective SDOF damping coefficient per leg |
| $C_{e\emptyset}$ | = | effective SDOF yaw damping coefficient |
| $D$ | = | diameter of the cylinder |
| $d'$ | = | effective water depth considering penetration |
| $f_{Nx}$ | = | surge natural frequency |
| $f_{Ny}$ | = | sway natural frequency |
| $f_{N\phi}$ | = | yaw natural frequency |
| $f_v$ | = | vortex shedding frequency of the cylinder |
| $f_O\,(z)$ | = | oscillatory excitation force distribution along leg |
| $f_{Ox}\,(z)$ | = | oscillatory drag force distribution along leg |
| $f_{Oy}\,(z)$ | = | oscillatory lift force distribution along leg |
| $F_d$ | = | oscillatory drag force |
| $F_{eL}$ | = | effective SDOF force excitation per leg |
| $I$ | = | yaw inertia |
| $k_L$ | = | structural wave number/mode shape of the leg |
| $K$ | = | stiffness of a linear mass spring cylinder |
| $K_\emptyset$ | = | yaw stiffness |

| | | |
|---|---|---|
| $L$ | = | length, effective leg length (from leg bottom to hull interface) |
| $M$ | = | leg mass distribution |
| $m^*$ | = | mass ratio (mass per displaced mass) of the cylinder. |
| $M$ | = | mass of a linear mass springs cylinder |
| $M_{eL}$ | = | effective SDOF mass per leg at the hull interface level |
| $M_{\emptyset O}$ | = | Amplitude of oscillatory yaw moment |
| $M_{e\emptyset L}$ | = | effective SDOF yaw excitation per leg |
| $M_{e\emptyset}$ | = | effective SDOF yaw excitation |
| $MF$ | = | Mode Factor |
| $m_{\emptyset}(z)$ | = | oscillatory yaw moment distribution along leg |
| $m\ (z)$ | = | mass distribution along leg |
| $Re$ | = | Reynolds Number |
| $r_{\emptyset}$ | = | yaw radius of gyration |
| $R_{\emptyset}$ | = | radial distance of the leg from yaw centre |
| $St$ | = | Strouhal number |
| $U$ | = | 2D steady flow or uniform current velocity |
| $V_{rx}$ | = | surge reduced velocity |
| $V_{ry}$ | = | sway reduced velocity |
| $V_{r\phi}$ | = | yaw reduced velocity |
| $x_o$ | = | amplitude of inline VIV response |
| $x_o(z)$ | = | inline VIV response amplitude variation along leg |
| $X_L$ | = | inline VIV response of leg in way of the hull interface |
| $y_o$ | = | amplitude of cross flow VIV response |
| $Y_L$ | = | cross flow VIV response of leg in way of the hull interface |

| | | |
|---|---|---|
| z | = | elevation w.r.t to the seabed, positive upwards; at the seabed |
| $\emptyset_O$ | = | amplitude of yaw response |
| $\emptyset_L$ | = | yaw VIV response in way of the hull interface |
| $\rho$ | = | density of the fluid |
| $\omega_N$ | = | natural angular frequency |
| $\omega_V$ | = | vortex sheding angular frequency |
| $\zeta$ | = | damping ratio |

# 8. References


Assi, G.R.S., Bearman, P.W., Meneghini, J.R., 2010. On the wake-induced vibration of tandem circular cylinders: the vortex interaction excitation mechanism. Journal of Fluid Mechanics 661, 365-401.

Barltrop, N.D.P., Adams, A.J., 1991. Dynamics of Fixed Marine Structures (Third Edition). Butterworth-Heinemann.

Bearman, P.W., 2011. Circular cylinder wakes and vortex-induced vibrations. Journal of Fluids and Structures 27 (5–6), 648-658.

Bennett Jr, W.T., Patel, R.K., 1989. Jack-up behavior in elevated condition: model test and computer simulation. SNAME, NJ.

Blevins, R.D., 2001. Flow-Induced Vibration, Reprint ed. Krieger Publishing Company, Florida.

Blevins, R.D., Burton, T.E., 1976. Fluid Forces Induced by Vortex Shedding. Journal of Fluids Engineering 98 (1), 19-24.

Blevins, R.D., Coughran, C.S., 2009. Experimental investigation of vortex-induced vibration in one and two dimensions with variable mass, damping, and Reynolds number. Journal of Fluids Engineering, Transactions of the ASME 131 (10), 1012021-1012027.

Cammaert, A.B., Hoving, J.S., Vermeulen, R., 2014. Experimental program for ice loads on an artic jack-up structure, HYDRALAB IV User Meeting, Lisbon, Portugal.

Chakrabarti, S., 2005. Physical Modelling of Offshore Structures, Handbook of Offshore Engineering, Volumes 1-2. Elsevier.

DNV.GL, 2017. DNVGL-RP-C205, Recommended Practice, Environmental Conditions and Environmental Loads. DNV GL AS, Oslo.

Fujarra, A.L.C., Rosetti, G.F., de Wilde, J., Gonçalves, R.T., 2012. State-of-Art on Vortex-Induced Motion: A Comprehensive Survey After More Than One Decade of Experimental Investigation. (44915), 561-582.

Gonçalves, R.T., Freire, C.s.M., Rosetti, G.F., Franzini, G.R., Fujarra, A.L.C., Meneghini, J.R., 2011a. Experimental Comparisons to Assure the Similarity Between VIM (Vortex-Induced Motion) and VIV (Vortex-Induced Vibration) Phenomena. (44397), 11-22.

Gonçalves, R.T., Fujarra, A.L.C., Rosetti, G.F., Kogishi, A.M., Koop, A., 2018. Experimental study of the column shape and the roughness effects on the vortex-induced motions of deep-draft semi-submersible platforms. Ocean Engineering 149, 127-141.

Gonçalves, R.T., Rosetti, G.F., Fujarra, A.L.C., Nishimoto, K., Oliveira, A.C., 2011b. Experimental Study on Vortex-Induced Motions (VIM) of a Large-Volume Semi-Submersible Platform. (44397), 1-9.

Govardhan, R., Williamson, C.H.K., 2004. Critical mass in vortex-induced vibration of a cylinder. European Journal of Mechanics - B/Fluids 23 (1), 17-27.

Grundlehner, G.J., 1997. Systematic model tests on a harsh environment jack-up in elevated condition. Marine Structures 10 (2–4), 159-180.

Han, Z., Zhou, D., He, T., Tu, J., Li, C., Kwok, K.C.S., Fang, C., 2015. Flow-induced vibrations of four circular cylinders with square arrangement at low Reynolds numbers. Ocean Engineering 96, 21-33.

Iwan, W.D., Blevins, R.D., 1974. A Model for Vortex Induced Oscillation of Structures. Journal of Applied Mechanics 41 (3), 581-586.

Jiang, R., 2012. FLOW-INDUCED VIBRATIONS OF TWO TANDEM CYLINDERS IN A CHANNEL. Thermal Science 16 (5), 1377-1381.

Johnson, T.L., Patel, R.K., 1992. The use of small scale physical models and numerical models for jack-up design, Recent Developments in Jack Up Platforms. Blackwell Scienific Publications, Oxford.

Journee, J., Massie, W., Boon, B., Onnink, R., 1988. Model experiments on jack-up platform hydrodynamics. TU Delft.

Khalak, A., Williamson, C.H.K., 1997a. FLUID FORCES AND DYNAMICS OF A HYDROELASTIC STRUCTURE WITH VERY LOW MASS AND DAMPING. Journal of Fluids and Structures 11 (8), 973-982.
Khalak, A., Williamson, C.H.K., 1997b. Investigation of relative effects of mass and damping in vortex-induced vibration of a circular cylinder. Journal of Wind Engineering and Industrial Aerodynamics 69–71 (0), 341-350.
King, R., Prosser, M.J., Johns, D.J., 1973. On vortex excitation of model piles in water. Journal of Sound and Vibration 29 (2), 169-188,IN161-IN162.
Liang, Y., Tao, L., Liu, M., Xiao, L., 2017. Experimental and Numerical Study on Vortex-Induced-Motions of a Dee-Draft Semi-Submersible Concept. Applied Ocean Research 67, 169-187.
Nicholls-Lee, R., Hindley, S., Parkinson, R., 2013. Development of an economic and efficient installation vessel for tidal stream energy converter arrays, International Conference on Offshore Mechanics and Arctic Engineering - OMAE. ASME, Nantes, France, p. 9.
PANEL OC-7, S.A.O.J.-U.R., 2008. Guidelines for Site Specific Assessment of Mobile Jack-Up Units, Technical and Research Bulletin. SNAME, p. 366.
Ramadasan, S., Tao, L., Dev, A., 2018. Antinode Fairings: An Optimum Solution for Reduction of Vortex Induced Vibration, Offshore Technology Conference Asia. Offshore Technology Conference, Kuala Lumpur, Malaysia.
Raven, P.W.J., Stuart, R.J., Bray, J.A., Littlejohns, P.S., 1985. Full-Scale Dynamic Testing of Submarine Pipeline Spans, Offshore Technology Conference. Offshore Technology Conference, Houston, Texas, p. 10.
Sainsbury, R.N., King, D., 1971. THE FLOW INDUCED OSCILLATION OF MARINE STRUCTURES. Proceedings of the Institution of Civil Engineers 49 (3), 269-302.
Sakai, T., Morishita, M., Iwata, K., Kitamura, S., 2002. Experimental Study on the Avoidance and Suppression Criteria for the Vortex-Induced Vibration of a Cantilever Cylinder. Journal of Pressure Vessel Technology 124 (2), 187-195.
Sarpkaya, T., 2004. A critical review of the intrinsic nature of vortex-induced vibrations. Journal of Fluids and Structures 19 (4), 389-447.
Sarpkaya, T., Isaacson, M., 1981. Mechanics of wave forces on offshore structures. Van Nostrand Reinhold Co.
Skop, R.A., Griffin, O.M., 1973. A model for the vortex-excited resonant response of bluff cylinders. Journal of Sound and Vibration 27 (2), 225-233.
Sumer, B.M., Fredsøe, J., 2006. Hydrodynamics around Cylindrical Structures (Revised Edition). World Scientific.
Sumner, D., 2010. Two circular cylinders in cross-flow: A review. Journal of Fluids and Structures 26 (6), 849-899.
Thake, J., 2005. Development, Installation and Testing of a Large-Scale Tidal Current Turbine Department of Trade and Industry, UK, p. 74.
Vandiver, J.K., 2012. Damping Parameters for flow-induced vibration. Journal of Fluids and Structures 35, 105-119.
Vickery, B.J., Watkins, R.D., 1964. FLOW-INDUCED VIBRATIONS OF CYLINDRICAL STRUCTURES A2 - SILVESTER, RICHARD, Hydraulics and Fluid Mechanics. Pergamon, pp. 213-241.
Wang, X.K., Gong, K., Liu, H., Zhang, J.X., Tan, S.K., 2013. Flow around four cylinders arranged in a square configuration. Journal of Fluids and Structures 43 (0), 179-199.
Williamson, C.H.K., Govardhan, R., 2004. VORTEX-INDUCED VIBRATIONS. Annual Review of Fluid Mechanics 36 (1), 413-455.
Zdravkovich, M.M., 1985. Flow induced oscillations of two interfering circular cylinders. Journal of

Sound and Vibration 101 (4), 511-521.
Zhao, M., Cheng, L., 2012. Numerical simulation of vortex-induced vibration of four circular cylinders in a square configuration. Journal of Fluids and Structures 31 (0), 125-140.

# 9. List of Tables



# 10. List of Figures